Int J Syst Assur Eng Manag (Jan-Mar 2012) 3(1):40–46
DOI 10.1007/s13198-012-0093-x

ORIGINAL ARTICLE

Broken rotor bars diagnosis in an induction motor fed from a frequency converter: experimental research

K. Yahia · A. J. M. Cardoso · S. E. Zouzou · S. Gueddidi

Received: 2 May 2011 / Revised: 16 February 2012 / Published online: 27 April 2012

Abstract Rotor electrical faults are common types of faults in squirrel cage induction motors (IMs) and have been investigated in detail under steady state conditions for direct mains-fed machines. Motor current signature analysis (MCSA) has been widely reported in the literature as a suitable fault diagnostic technique for directly-supplied IMs. However, when an induction motor is fed from a frequency converter composed of a rectifier, DC link filter and a PWM inverter, its characteristic signals (currents, voltages, electromagnetic torque, etc.) become very noisy. This paper presents an experimental analysis of a damaged squirrel cage induction motor supplied from an industrial frequency converter at different speed and load levels. The main purpose is to experimentally study the ability of the MCSA to diagnose the occurrence of broken rotor bars under these operating conditions.

K. Yahia · S. E. Zouzou · S. Gueddidi
Electrical Engineering Laboratory, Department of Electrical Engineering, University of Biskra, Biskra, Algeria

K. Yahia (✉) · A. J. M. Cardoso
Department of Electrical and Computer Engineering, Instituto de Telecomunicações, University of Coimbra, Pólo 2, 3030-290 Coimbra, Portugal
e-mail: kdyahia@mail.co.it.pt

A. J. M. Cardoso
e-mail: ajmcardoso@ieee.org

A. J. M. Cardoso
Department of Electromechanical Engineering, University of Beira Interior, Calçada Fonte do Lameiro, 6201-001 Covilha, Portugal

Keywords Induction motor · Frequency converter · Broken rotor bars fault diagnosis · Motor current signature analysis (MCSA)

1 Introduction

Induction motors (IMs) are the most widely used electrical machines because they are generally reliable and require minimum maintenance. With the development of power electronics and microprocessors, they are predominantly fed from pulse width modulation (PWM) converters for variable speed operation. PWM frequency converters are designed to vary the speed of IMs by supplying a variable voltage/variable frequency output. Each converter achieves this in three basic steps. First, it converts the user supplied sine-wave power to a fixed DC voltage, usually through a diode bridge full wave rectifier. Second, this fixed DC voltage is smoothed by some bus capacitors and in some cases bus reactors. Third, and most critical, the fixed DC potential is inverted by a series of output switching devices, usually transistors, into a series of pulses that simulate a sine-wave at the motor terminals. The number of variable speed applications controlled by means of a frequency converter has increased significantly over the recent years. This may be explained by the many benefits provided by such applications, such as aloof control, cost reduction, gain of productivity, energy efficiency, versatility and high quality of control (Technical guide 2008). However, some effects must be considered when applying frequency converters to inductions motors, such as overload motor current (due to excessive voltage harmonics, improper V/Hz levels or increased loading), excessive motor temperature (due to insufficient cooling, excessive torque level, reduced

motor efficiency, increased power requirements, …), insufficient motor starting torque (due to reduced V/Hz level, …), mechanical failure of the motor or associated coupling components (due to torque pulsations, …), winding damage or premature failure (due to repetitive high transient voltages, fast rate of voltage rise or excessive switching rates), induced shaft voltages which can cause circulating currents harmful to the bearings and excessive motor noise level (due to increased fan noise, excitation of mechanical resonant points, or magnetic noise caused by PWM waveforms) (Bonett 1996; Besnerais et al. 2010). The magnetic noise level increase is caused by the harmonic content of the PWM waveforms. This harmonic content depends strongly on the used technique for the control of the inverter and the chosen switching frequencies. Higher switching frequencies can help to minimize the motor noise; unfortunately these higher switching frequencies can also create additional dielectric stress on the insulation system as previously described (Bonett 1996). Using newer topologies of inverters and their control techniques can also decrease the noise level of the motor (Lo et al. 2000; Ruiz-González et al. 2010).

The predictive maintenance of IMs fed from frequency converters becomes necessary in order to avoid plant downtime, revenue losses and even damage to other equipment and personnel. Motor current signature analysis (MCSA) is one of the most widely used techniques for fault detection in induction machines. It is based on fast fourier transform (FFT). The MCSA was intensively studied in the past for the broken rotor bars (BRBs) detection in mains-fed IMs (Kliman and Stein 1992; Thomson and Fenger 2001; Bellini et al. 2001; Jung et al. 2006). This method is based on the measurement of sidebands in the stator current spectrum, which are usually located close to the supply frequency component, for BRBs fault (Kliman and Stein 1992).

The use of frequency converters introduces some new problems in IMs fault diagnosis. In fact, some additional harmonics will be induced in the current spectrum (Villada et al. 2003; Sotelo et al. 2010, Uddin et al. 2010) which complicate the fault detection task. Therefore, the subject of inverter-fed IMs fault diagnosis has been also addressed in the literature using MCSA as well as other alternative methods. In (Cruz and Cardoso 1999), the Extended Park's Vector Approach (EPVA) was proposed for rotor cage fault diagnosis in voltage source inverter fed IMs, and it was shown that BRBs can be effectively diagnosed through this method. Stator windings fault detection in induction machines fed from power converters using high-frequency negative-sequence currents was also proposed in (Briz et al. 2009). Bearing and eccentricity fault diagnosis in three-phase IMs driven by voltage source inverters have been also reported in the literature (Duque et al. 2005; Akin et al. 2007, 2008; Sotelo et al. 2010). In (Sotelo et al. 2010), eccentricity in IMs fed by mains and frequency converter using stator line current spectral analysis has been investigated. It has been shown that fault detection in converter-fed IMs presents some additional problems as compared to a sinusoidal supply situation, due to the produced noise and the generated harmonic content. This paper presents an experimental analysis of a faulty induction motor driven by a frequency converter with an open-loop constant V/Hz control. According to this strategy, the motor speed is properly adjusted by changing the stator supply frequency, while keeping constant the voltage/frequency ratio. The main purpose of this paper is to experimentally study the ability of the MCSA to diagnose the occurrence of BRBs under different speed and load levels. The present paper consists of the following sections: an introduction (Sect. 1), a description of BRBs in IMs (Sect. 2), the experimental test rig (Sect. 3), experimental results presentation (Sect. 4) and finally the two last sections are the conclusions and references.

2 BRBs in IMs

If symmetrical three-phase stator windings of a three-phase induction motor are supplied by a symmetrical three-phase voltage system, a rotating magnetic field is induced in its air gap. This field rotates at a synchronous speed with respect to the stator. In the case of a symmetrical machine, a backward rotating component does not exist. Stator rotating magnetic field induces EMFs and currents in the rotor windings with a frequency $f_2 = s{\cdot}f_1$ where, $s$and f_1 are the slip and the supply frequency, respectively. Those currents induce a rotor rotating magnetic field which rotates at a speed $n_s{\cdot}s$ with respect to the rotor, where n_s is the synchronous speed. In the case of a symmetric rotor winding, only a direct component of the current exists. If any kind of asymmetry occurs in the rotor cage (for example, BRBs) backward components will be induced, which rotate at a slip frequency with respect to the rotor, but in the opposite direction. Consequently, an EMF will be induced in the stator windings at a frequency given by (Bellini et al. 2001; Thomson and Fenger 2001):

$$f_{lbrb} = (1 - 2s)f_1 \quad (1)$$

These current oscillations cause torque and speed oscillations at twice slip frequency $2sf_1$ (Uddin et al. 2010). Speed oscillation also depends on motor and drive inertia. Speed oscillation reduces the magnitude of the $f_{lbrb} = (1 - 2s)f_1$ component, but the upper component at $f_{ubrb} = (1 + 2s)f_1$ is induced as well. The upper component is enhanced by the third-time harmonic of the flux (Thomson and Fenger 2001). Therefore, BRBs induce

sidebands in the stator current at frequencies given by (Bellini et al. 2001; Kliman and Stein 1992):

$$f_{brb} = (1 - 2s)f_1 \quad (2)$$

On-line detection of BRBs can therefore be based on the spectrum analysis of current or electromagnetic torque signals in order to determine the lower and upper frequency sidebands $(1 \pm 2s)f_1$ around the fundamental current frequency component or the $2sf_1$ twice slip frequency components in the electromagnetic torque spectrum.

3 Experimental test rig

The experimental test rig is shown in Fig. 1. The main components of the test rig are as follows:

- Three-phase, 380 V, 50 Hz, 6.40 A, Y connection, 4-pole, 28 bars, 21 Nm, 1,440 rpm, 3 kW Leroy Somer squirrel cage induction motor.
- DC generator coupled to the induction motor to provide an adjustable load.
- Torque-meter inserted between the induction motor and the DC generator for torque sensing.
- Mechanical couplings between the induction motor and the DC generator.
- Variable-resistor bank as a variable load of the DC generator; the load of the DC generator and, consequently, the induction motor can be adjusted by varying this resistance and/or regulating the excitation current of the generator through a variable resistor.
- Hitachi frequency converter for induction motor drive systems type L200-055HFEF/HFU with rating values in accordance with that of the induction motor. This drive has been mainly designed for closed-loop scalar or vector control of the motor, but the user can also utilize it as an open-loop scalar control in the constant voltage/frequency (V/Hz) method.

Fig. 1 View of the experimental test rig

Fig. 2 The used rotors

- PC equipped with dSpace card type 1104, enabling the use of three sampled line currents i_a, i_b and i_c, three voltages v_a, v_b and v_c, and torque signals.

Three different rotors were used in the experiments: a healthy one and two others with one and two BRBs, respectively (Fig. 2).

4 Experimental results

4.1 Motor current spectra

Figures 3, 4, and 5 show the stator line currents and their corresponding spectra for a healthy induction motor directly-supplied from the mains and from a frequency converter at 80 and 20 % of rated load, respectively. A switching frequency of 12 kHz was chosen for the PWM control. A sampling frequency of 10 kHz was also chosen for acquiring the motor currents, voltages and electromagnetic torque data. Hence, 100,000 samples were obtained with 0.1 Hz as frequency resolution. It is noticed that the spectral analysis of currents confirms the healthy state condition of the motor by the absence of sideband components $(1 \pm 2s)f_1$.

The presence of $(1 \pm 2s)f_1$ sideband components in the spectra of Figs. 6 and 7 for (a) a mains-fed induction motor and (b) a converter-fed one demonstrate the existence of BRBs, especially at 80 % of rated load, where it is obvious an important increase of the $(1 \pm 2s)f_1$ sideband components as compared to the healthy state. This increase is more pronounced in the case of 80 % of rated load.

Figure 8 shows the stator current spectra for an induction motor driven with a 30 Hz output frequency converter: (a) with 20 % of rated load and (b) with 80 % of rated load. From the stator current spectra analysis it can concluded that the MCSA is still effective as a diagnostic

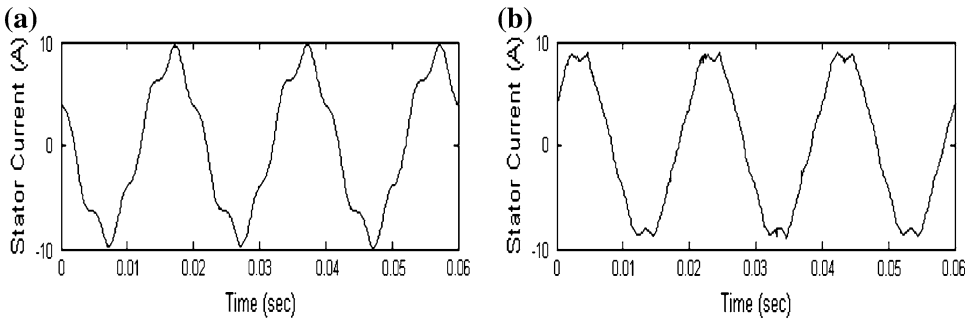

Fig. 3 Stator line current time-domain waveforms for a healthy motor with 80 % rated load: **a** mains-fed; **b** converter-fed

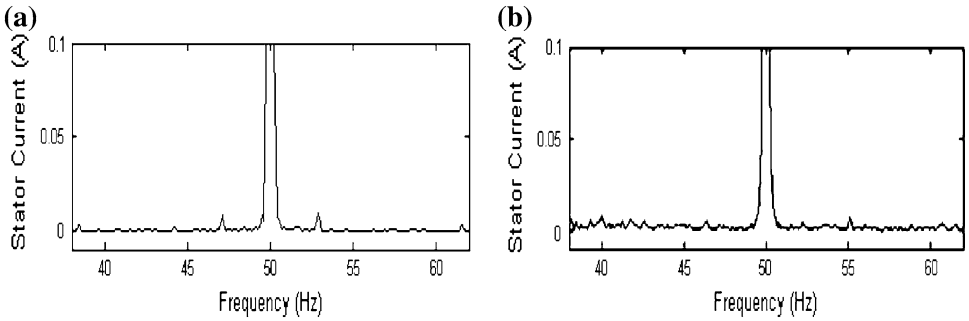

Fig. 4 Stator line current spectra for a healthy motor with 80 % rated load: **a** mains-fed ($s = 2.8$ %); **b** converter-fed ($s = 2.9$ %)

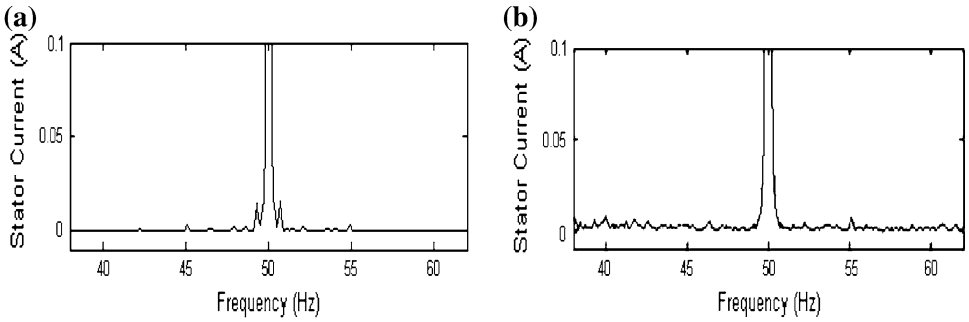

Fig. 5 Stator current spectra for a healthy motor with 20 % rated load: **a** mains-fed ($s = 0.8$ %); **b** converter-fed ($s = 0.8$ %)

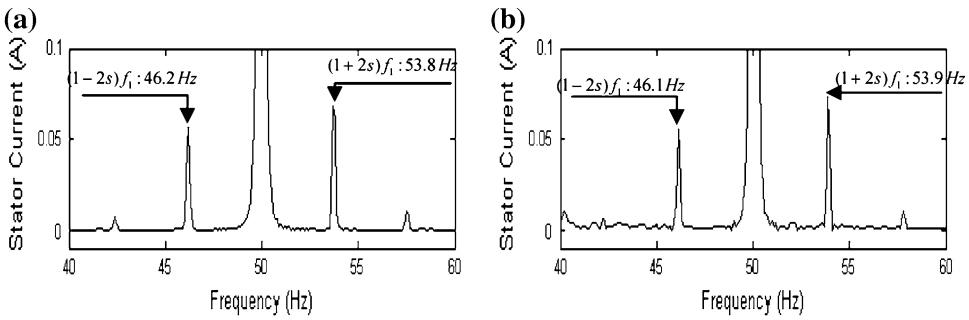

Fig. 6 Stator current spectra for the case of one broken bar, with 80 % rated load: **a** mains-fed ($s = 3.8$ %); **b** converter-fed ($s = 3.9$ %)

technique for this speed range. The lower and upper sideband components are clearly shown at 28 and 32 Hz, respectively.

The current spectra for a 10 Hz output frequency converter for 80 and 20 % rated load are presented in Fig. 9a, b, in which the $(1 \pm 2s)f_1$ sideband components cannot be observed.

They are overlapped by the mains frequency at 10 Hz. The diagnosis becomes very difficult in this speed range.

Being the amplitude of the $(1 \pm 2s)f_1$ sideband components directly related with the extension of the fault, a severity factor (SF)—defined as the ratio of $(1 \pm 2s)f_1$ amplitudes sum and the main component at f_1—can be used to evaluate the extension of the fault and the effectiveness of the MCSA at different speed ranges (Bellini et al. 2001). Table 1 and Fig. 10 show the numerical values and the SF evolution, respectively. It can be concluded that this SF gives results in accordance with

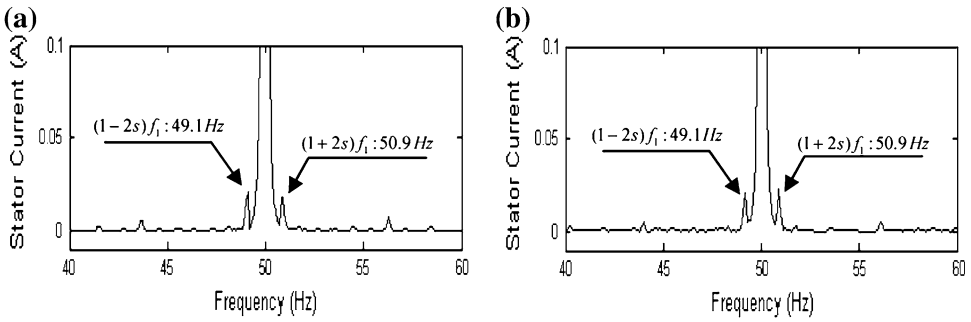

Fig. 7 Stator current spectra for the case of one broken bar, with 20 % rated load: **a** mains-fed ($s = 0.9$ %); **b** converter-fed ($s = 0.9$ %)

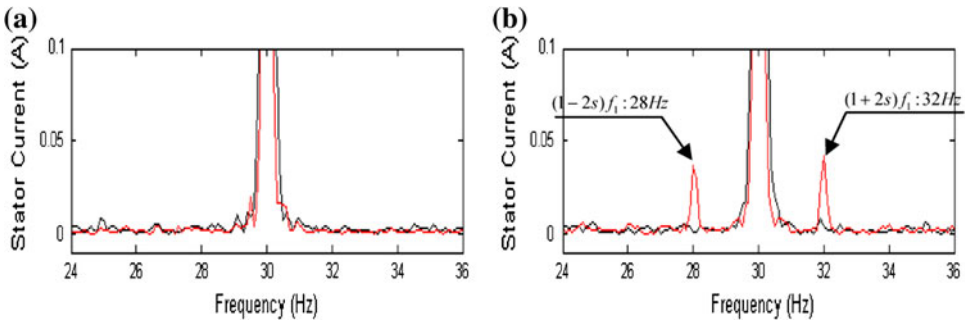

Fig. 8 Stator current spectra for the case of 30 Hz of frequency converter output: **a** 20 % rated load ($s = 0.83$ %); **b** 80 % rated load ($s = 3.33$ %). *Black line*: healthy rotor; *red line*: one broken rotor bar. (Color figure online)

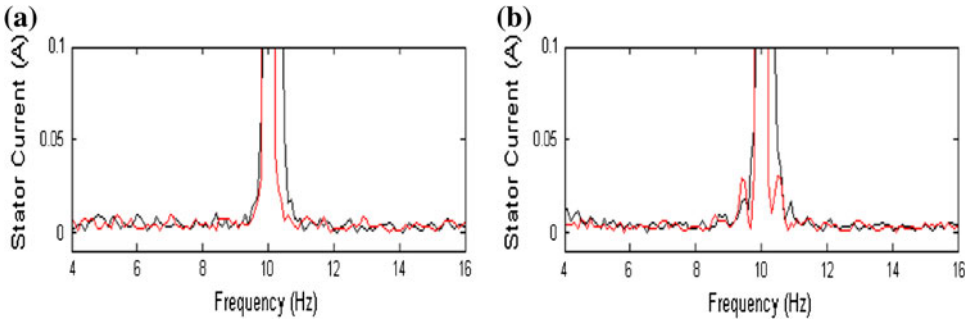

Fig. 9 Stator current spectra for the case of 10 Hz of frequency converter output: **a** 20 % rated load; **b** 80 % rated load. *Black line*: healthy rotor; *red line*: one broken rotor bar. (Color figure online)

Table 1 SF for different speed and load levels for the case of one broken rotor bar

Load (%)	10 Hz (%)	20 Hz (%)	30 Hz (%)	40 Hz (%)	50 Hz (%)
20	0.39	0.6	0.79	0.88	1
80	0.92	1	1.24	1.51	1.53

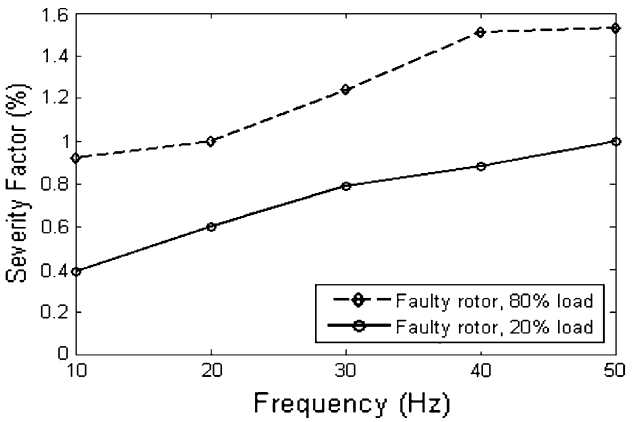

Fig. 10 SF for different speed and load levels for the case of one broken rotor bar

the theory, for the case of a broken rotor bar, e.g. the SF increases with the load and speed. Obviously, the SF also increases with the motor fault extension.

For example, at 10 Hz, the SF increases from 0.24 % for the healthy state to 0.39 % for the case of one broken rotor bar at 20 % rated load and from 0.58 % for the healthy state to 0.92 % for the case of one broken rotor bar at 80 % rated load.

4.2 Motor electromagnetic torque spectra

In this section, the results of motor electromagnetic torque spectral analysis are presented for a healthy motor at 80 % rated load (Fig. 11), faulty motor with one broken rotor bar at 80 % rated load (Fig. 12) and faulty motor with one broken rotor bar at 20 % rated load (Fig. 13). In all cases,

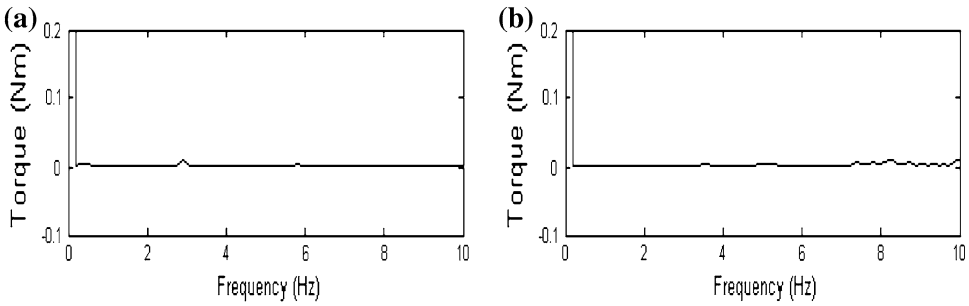

Fig. 11 Electromagnetic torque spectra for a healthy motor, with 80 % rated load and 50 Hz of frequency converter output, **a** mains-fed ($s = 2.8$ %), **b** converter-fed ($s = 2.9$ %)

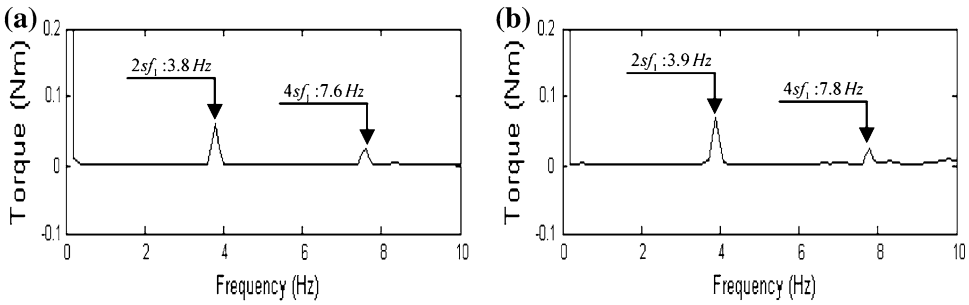

Fig. 12 Electromagnetic torque spectra for the case of one broken bar, with 80 % rated load and 50 Hz of frequency converter output, **a** mains-fed ($s = 3.8$ %); **b** converter-fed ($s = 3.9$ %)

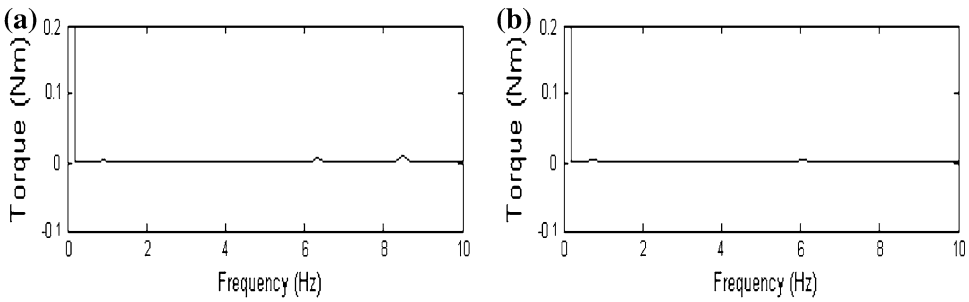

Fig. 13 Electromagnetic torque spectra for the case of one broken bar, with 20 % rated load and 50 Hz of frequency converter output, **a** mains-fed ($s = 0.9$ %), **b** converter-fed ($s = 0.9$ %)

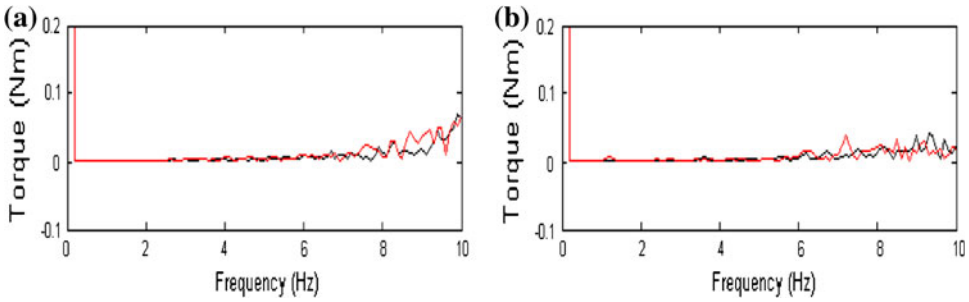

Fig. 14 Electromagnetic torque spectra with 20 Hz of frequency converter output: **a** 20 % rated load ($s = 1.75$ %), **b** 80 % rated load ($s = 3.25$ %). *Black line*: healthy rotor; *red line*: one broken rotor bar. (Color figure online)

(a) refers to a mains-fed machine and (b) to a converter-fed one. The aim is to analyze the $2sf_1$ component in the electromagnetic torque spectra. Figure 11, does not present any relevant components which confirms the healthy state of the machine. In Fig. 12a $2sf_1$ and $4sf_1$ components at 3.8 and 7.6 Hz are presented for the case of a mains-fed machine, while $2sf_1$ and $4sf_1$ components at 3.9 and 7.8 Hz are also presented in Fig. 12b for the case of a converter-fed machine. These components are clearly visible and they demonstrate the faulty state condition of the motor.

Figure 13a, b presents the electromagnetic torque spectra for the cases of an induction motor fed from the mains and from a frequency converter, respectively, at 20 % rated load, where the $2sf_1$ components are not visible for this load level.

Figure 14 presents the electromagnetic torque spectra for the induction motor driven at 20 Hz of frequency converter output. The observation of the $2sf_1$ component is very difficult and the broken rotor bar diagnosis becomes impossible for this speed range.

5 Conclusions

The work presented in this paper deals with the application of the spectral analysis of current and electromagnetic torque for an induction motor driven by an industrial frequency converter. The experimental work was performed for different speed levels (from 10 to 50 Hz) and with a frequency converter working in an open-loop V/Hz control. From the experimental results, it was concluded that BRBs diagnosis via the current and electromagnetic torque spectra analysis is very difficult at low speeds (especially at speeds less than 20 Hz), since the current and torque signals are very noisy and an overlap effect occurs in the spectra. Using a switching frequency lower than the chosen one (12 kHz) will even increase the diagnosis difficulties and the use of other diagnostic approaches and/or advanced signal processing techniques is therefore necessary.

Acknowledgments The authors would like to thank Mr. M. Sahraoui of the Electrical Engineering Laboratory of the University of Biskra for his role in the laboratory tests.

References

Akin B, Toliyat HA, Orguner U, Rayner M (2007) PWM inverter harmonics contributions to the inverter-Fed induction machine bearing fault diagnosis. IEEE, 22nd annual applied power electronics conference, Anaheim, CA, pp 1393–1399

Akin B, Orguner U, Toliyat HA, Rayner M (2008) Low order PWM inverter harmonics contributions to the inverter-fed induction machine fault diagnosis. IEEE Trans Ind Electron 55(2):610–619

Bellini A, Fillippetti F, Franceschini G, Tassoni C, Kliman G (2001) Quantitative evaluation of induction motor broken bars by means of electrical signature analysis. Trans Ind Electron 37(5):1248–1255

Besnerais JL, Lanfranchi V, Hecquet M, Brochet P (2010) Characterization and reduction of audible magnetic noise due to PWM supply in induction machines. IEEE Trans Ind Electron 57(4):1288–1295

Bonett AH (1996) Analysis of the impact of pulse-width modulated inverter voltage waveforms on AC induction motors. IEEE Trans Ind Appl 32(2):386–392

Briz F, Degner MW, Guerrero JM, García P (2009) Stator windings fault diagnostics of induction machines operated from inverters and soft-starters using high-frequency negative-sequence currents. IEEE Trans Ind Appl 45(5):1637–1646

Cruz SMA, Cardoso AJM (1999) Rotor cage fault diagnosis in voltage source inverter fed induction motors, by the extended park's vector approach. IEEE international symposium on diagnostics for electrical machines, power electronics and drives, Gijón, Spain, pp 105–110

Duque O, Pérez M, Morinigo D (2005) Detection of bearing faults in cage induction motors fed by frequency converter using spectral analysis of line current. IEEE International Conference on Electric Machines and Drives, San Antonio, pp 17–22

Jung JH, Lee JJ, Kwon BH (2006) Online diagnosis of induction motors using MCSA. IEEE Trans Ind Electron 53(6):1842–1852

Kliman GB, Stein J (1992) Methods of motor currents signature analysis. Electr Mach Power Syst 20(5):463–474

Lo WC, Chan CC, Zhu ZQ, Lie X, Howe D, Chau KT (2000) Acoustic noise radiated by PWM-controlled induction machine drives. IEEE Trans Ind Electron 47(4):880–889

Ruiz-González A, Meco-Gutiérrez MJ, Pérez-Hidalgo F, Vargas-Merino F, Heredia-Larrubia JR (2010) Reducing acoustic noise radiated by inverter-fed induction motors controlled by a new PWM strategy. IEEE Trans Ind Electron 57(1):228–236

Sotelo DM, Escudero LAG, Perez OD, Alonso MP (2010) Practical aspects of mixed-eccentricity detection in PWM voltage-source-inverter-fed induction motors. IEEE Trans Ind Electron 57(1):252–262

Technical guide (2008) Induction motors fed by PWM frequency inverters. http://www.weg.net/. Assessed 12 Jan 2012

Thomson WT, Fenger M (2001) Current signature analysis to detect induction motors faults. IEEE Ind Appl Mag 7(4):26–34

Uddin MN, Wang W, Huang ZR (2010) Modeling and minimization of speed ripple of a faulty induction motor with broken rotor bars. IEEE Trans Ind Electron 46(6):2243–2250

Villada F, Cadavid D, Munoz N, Valencia D, Parra D (2003) Fault diagnosis in induction motors fed by PWM inverters. IEEE international symposium on diagnostics for electric machines, power electronics and drives, Atlanta, CA, pp 24–26